



Available online at www.sciencedirect.com



C. R. Mecanique 332 (2004) 231–236



Experimental observation of the straining field responsible for vortex ring instability

Antoine Dazin, Patrick Dupont, Michel Stanislas *

Laboratoire de mécanique de Lille, boulevard Paul Langevin, cité Scientifique, 59655 Villeneuve d'Ascq, France

Received 25 November 2003; accepted 2 December 2003

Presented by Pierre Perrier

Abstract

The aim of this work is to show experimentally the straining field responsible for the vortex ring instability. To do so, the velocity field in the neighbourhood of the core is measured with Particle Image Velocimetry. This field is compared with the one coming from theoretical work on a thin vortex ring in an ideal fluid. Theoretical and experimental data fit well. This indicates that the linear phase of the instability is weakly influenced by viscosity. *To cite this article: A. Dazin et al., C. R. Mecanique 332 (2004).*

© 2004 Académie des sciences. Published by Elsevier SAS. All rights reserved.

Résumé

Observation expérimentale du champ responsable de l'instabilité du tourbillon torique. L'objectif de ce travail est de mettre en évidence expérimentalement le champ en point-selle responsable de l'instabilité du tourbillon torique. Pour cela, le champ à proximité du noyau issu des mesures par Vélocimétrie par Images de Particules est comparé à celui établi théoriquement pour des tourbillons à petits noyaux en fluide idéal. Les données théoriques et expérimentales étant assez proche, il est possible d'utiliser les premières pour comprendre les seconds. Le champ en point-selle responsable de l'instabilité est ensuite mis en évidence dans des résultats expérimentaux. *Pour citer cet article : A. Dazin et al., C. R. Mecanique 332 (2004).*

© 2004 Académie des sciences. Published by Elsevier SAS. All rights reserved.

Keywords: Fluid mechanics; Vortex ring instability; Particle Image Velocimetry

Mots-clés : Mécanique des fluides ; Instabilité du tourbillon torique ; Vélocimétrie par Images de Particules

Version française abrégée

Un tourbillon torique se réalise très simplement en poussant du fluide à travers un orifice circulaire. Il est donc devenu un sujet d'étude classique de la Mécanique des Fluides. Son instabilité a été clairement mise en évidence expérimentalement [1,2]. Les modèles théoriques [3–5] prévoient correctement les premiers phénomènes instables.

* Corresponding author.

E-mail address: stanislas@ec-lille.fr (M. Stanislas).

D'après ces travaux, l'instabilité résulte de la présence d'un champ de contrainte, en point-selle, centré sur le noyau du tourbillon. La détermination théorique du champ de vitesse pour des tourbillons à petits noyaux en fluide idéal [4] met en évidence sa présence. L'objectif de ce travail est de mettre ce champ en évidence expérimentalement à l'aide de mesure par Vélocimétrie par Images de Particules.

Les tourbillons sont obtenus par une décharge de fluide à travers un tube cylindrique (de diamètre $D_p = 35$ mm) plongé dans l'eau d'un aquarium (Fig. 1). Deux types de tourbillon ont été utilisés. Leur caractéristiques sont reportées dans le Tableau 1. Des mesures de P.I.V. ont été effectuées dans un plan de symétrie du tourbillon torique (Fig. 1). L'incertitude de mesure sur chacun des vecteurs a été estimée à moins de 5 %.

Ces mesures ont été extraites dans un repère polaire centré sur l'un des noyaux du tourbillon (Fig. 2). Ces résultats sont comparés au champ théorique déterminé donné par l'Eq. (3).

La comparaison des vitesses radiales et azimutales (Figs. 3 et 4) en fonction de φ montre une bonne correspondance entre les résultats théoriques et expérimentaux. On retrouve dans les résultats les effets des termes d'ordre 0, 1 et 2 en $\varepsilon = a/R$. (Ces derniers sont dus au champ en point-selle.)

Les résultats théoriques et expérimentaux étant assez proche, il est possible d'utiliser les seconds pour comprendre les premiers. La Fig. 5(a) présente le résultat de l'opération {[Champ total expérimental] – [(Champ théorique)₀ + (Champ théorique)₁]}. Le champ obtenu est similaire au champ à l'ordre 2 de l'Eq. (3) (Fig. 5(b)), bien que plus bruité, puisqu'il est perturbé par le bruit de mesure.

On valide ainsi expérimentalement, pour des tourbillons à gros noyaux, en fluide réel, le champ de vitesse issu des calculs théoriques en fluide idéal pour des tourbillons à petits noyaux. Cela nous a permis de mettre en évidence, sur des résultats expérimentaux, la champ en point-selle responsable de l'instabilité et de démontrer ainsi que la phase linéaire de l'instabilité est faiblement influencée par la viscosité.

1. Introduction

Generating a vortex ring is fairly easy. It can be done by pushing fluid through a cylindrical nozzle. It is thus a classical subject of study in Fluid Mechanics. The instability of the vortex ring was evidenced experimentally by Maxworthy [1] and Widnall et al. [2]. The theoretical models (Widnall et al. [3], Widnall and Tsai [4], Saffman [5]), based on linearized equations, predict correctly the first unstable mode. According to these theories, the vortex ring is unstable because of a straining field centered on the vortex core. The velocity field in the neighborhood of the core, calculated for thin vortices in an ideal fluid by Widnall and Tsai [4] shows the presence of this field. The aim of the present work is to compare this result to experimental data obtained with the help of Particle Image Velocimetry in order to show experimentally the straining field.

2. Experimental set-up

The experiments are performed in water. The vortex rings are generated by pushing fluid throughout the cylindrical nozzle of a pipe, which is plunged into an aquarium (2.4 m × 0.6 m × 0.6 m). The inner diameter of the pipe is $D_p = 35$ mm. The pipe is connected to a pressurised tank. Between the pipe and the tank, an electromagnetic valve opens the circuit for an adjustable duration. A polystyrene piston is fitted into the pipe in order to isolate the flow in the aquarium from the perturbations of the generating system. The stroke of this piston is adjustable. By setting the tank pressure and the opening time of the valve, it is possible to control the velocity of the piston (Fig. 1). Table 1 gives the characteristics of the two vortices produced for the present experiments (stroke to nozzle-diameter ratio and Reynolds number).

2D2C PIV records were obtained in the symmetry plane of the vortex ring. The laser sheet was generated with a 2 × 300 mJ BMI pulsed YAG laser. The PIV images were recorded with a CCD camera (Pulnix TM-9701, 768 × 484 pixels, 30 Hz framing rate), placed on one side of the aquarium. For the analysis of the PIV records, the

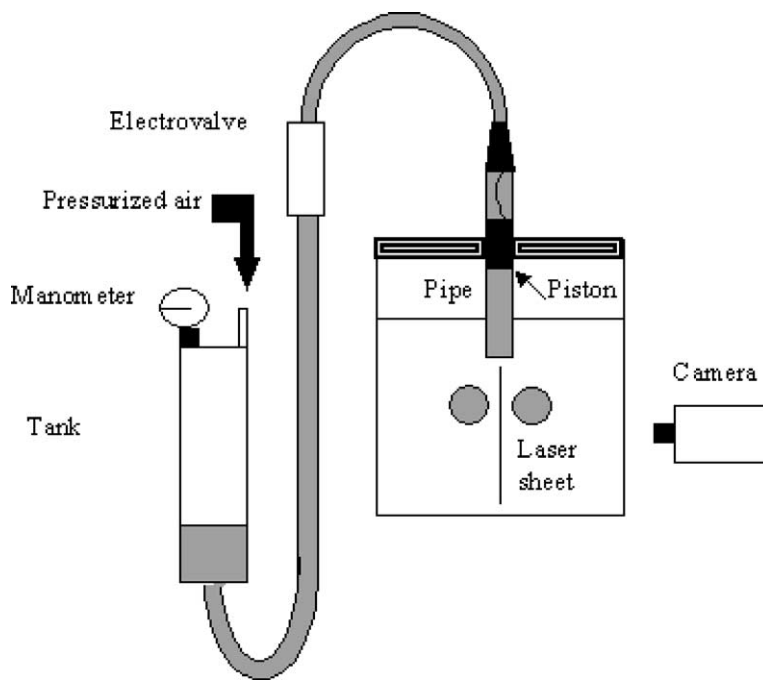


Fig. 1. Experimental set-up.

Fig. 1. Dispositif expérimental.

Table 1
Vortex characteristics
Tableau 1
Caractéristiques des tourbillons

	A'	C'
U_p (mm/s)	100	132
L_p/D_p	1.25	1.9
Re_p	3500	4600

cross-correlation technique was used with a correlation window size of 32×32 pixels (2D2C PIV). Correlation peaks were fitted with a three points Gaussian model. The results consist of fields of 48×26 velocity vectors with a temporal resolution of 15 fields per second. The field of view is 195×150 mm 2 . The measurement uncertainty was determined from a quiescent flow. It gives $\varepsilon_{rms} \approx 0.075$ pixel that is about 1% of the velocity. By taking into account the classical parameters having an influence on PIV accuracy (particle size and density, loss of particles, gradient of velocity), the uncertainty in the velocity measurement is less than 5% for the present experiments.

3. Comparison between experimental and theoretical velocity fields

3.1. Experimental data

In order to compare theoretical predictions and experimental results, velocities are extracted from experimental fields in a polar coordinate system centered on the vortex core (Fig. 2).

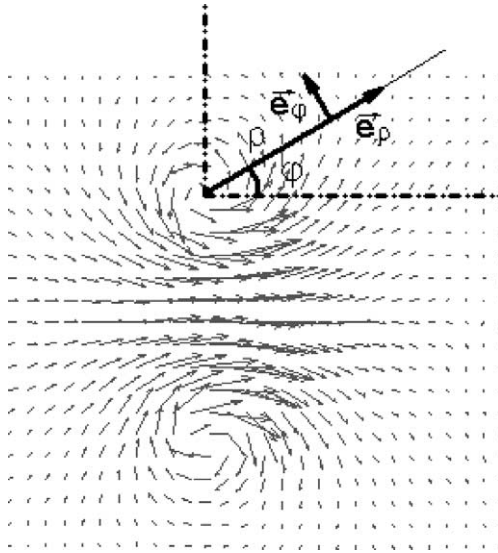


Fig. 2. Polar coordinate system.

Fig. 2. Repère polaire.

3.2. Theoretical data

The velocity field near the vortex core (for thin core vortex in an ideal fluid) is given by Widnall and Tsai [4]. Eq. (1) gives the velocity potential outside the core, in polar coordinates:

$$\begin{aligned} \Phi = & \varphi + \varepsilon \left(\frac{1}{8} \rho - \frac{3}{8\rho} - \frac{1}{2} \rho \ln \rho \right) \cos \varphi \\ & + \varepsilon^2 \left[\frac{5}{32} \rho^2 - \frac{9}{32\rho^2} + \frac{3}{32} + \frac{3}{16} \rho^2 \ln \rho - \frac{3}{16} \ln \frac{8}{\varepsilon} \left(\rho^2 - \frac{1}{\rho^2} \right) \right] \sin 2\varphi + \dots \end{aligned} \quad (1)$$

The ρ coordinates are scaled with the core radius a , and the velocities by $\Gamma/(2\pi a)$. Deriving this potential gives the radial and tangential velocity components. The translation speed of the vortex is added to these results because the theoretical coordinates system moves with the vortex on the contrary to the experimental one. This translation speed is given by Fraenkel [6]:

$$V = \frac{\Gamma}{4\pi R} \left[\log 8\varepsilon - \frac{1}{4} + O(\varepsilon \ln \varepsilon) \right] \quad (2)$$

with R the ring radius and $\varepsilon = a/R$. Finally the two velocity components are given by (3):

$$\begin{cases} u_{\rho\text{théo}} = 0 + \varepsilon \left[\left(-\frac{3}{8} + \frac{3}{8\rho^2} - \frac{1}{2} \ln \rho \right) + \frac{1}{2} \left(\ln \frac{8}{\varepsilon} - \frac{1}{4} \right) \right] \cos \varphi \\ \quad + \varepsilon^2 \left[\frac{1}{2} \rho + \frac{9}{16\rho^3} + \frac{3}{8} \rho \ln \rho - \frac{3}{8\rho} \ln \frac{8}{\varepsilon} \left(\rho^2 + \frac{1}{\rho^2} \right) \right] \sin 2\varphi \\ u_{\theta\text{théo}} = \frac{1}{\rho} + \varepsilon \left[\left(-\frac{1}{8} + \frac{3}{8\rho^2} + \frac{1}{2} \ln \rho \right) - \frac{1}{2} \left(\ln \frac{8}{\varepsilon} - \frac{1}{4} \right) \right] \sin \varphi \\ \quad + \varepsilon^2 \left[\frac{5}{16} \rho - \frac{9}{16\rho^3} + \frac{3}{8} \rho \ln \rho + \frac{3}{16\rho} - \frac{3}{8\rho} \ln \frac{8}{\varepsilon} \left(\rho^2 - \frac{1}{\rho^2} \right) \right] \cos 2\varphi \end{cases} \quad (3)$$

3.3. Comparison

Fig. 3 shows radial velocity component as a function of φ for an A' vortex. Experimental and theoretical results fit well. Moreover, we can clearly see the influence of the first order term which is in $\cos \varphi$ and of the second order one in $\sin 2\varphi$. Their effects are additive when $\varphi < 0$ and are competing when $\varphi > 0$.

Fig. 4 shows the tangential velocity component as a function of φ . Experimental and theoretical results agree also well. The velocities are always positive because the lowest order term (which is dominant) is positive. On top of that, we can find the first order ($\sin \varphi$) and the second order term ($\cos 2\varphi$) whose effects are adding when $\varphi < 0$ and competing when $\varphi > 0$.

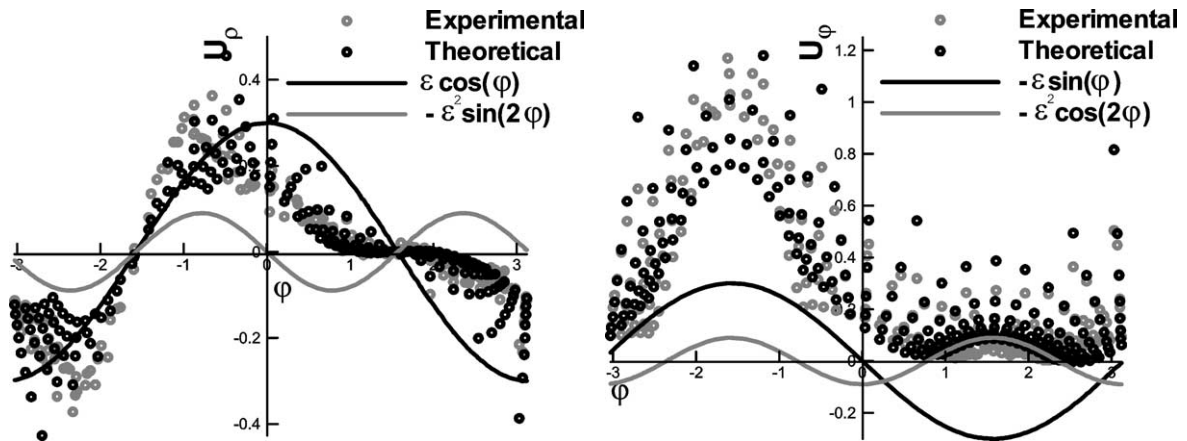


Fig. 3. Radial velocities as a function of φ .

Fig. 3. Vitesses radiales en fonction de φ .

Fig. 4. Tangential velocities as a function of φ .

Fig. 4. Vitesses azimuthales en fonction de φ .

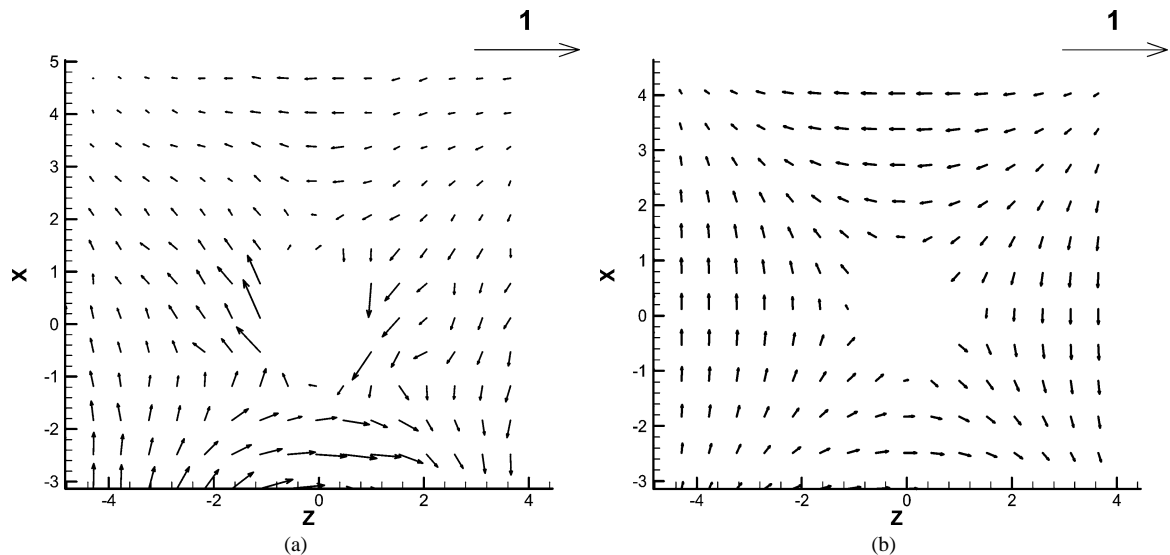


Fig. 5. (a) Experimental and (b) theoretical straining field.

Fig. 5. Champ en point-selle (a) expérimental et (b) théorique.

4. Straining field

The above results give the hope to show the straining field in the experimental results because:

- theoretical and experimental results are similar. It is thus possible to use the first to understand the second;
- the effects of the straining field are visible, although they correspond to the second order term in Eq. (3).

The result of the operation $\{[\text{Experimental field}] - [(\text{Theoretical field})_0 + (\text{Theoretical field})_1]\}$ is reported in Fig. 5(a). This field is similar to the second order field of Eq. (3) (Fig. 5(b)), that is the saddle point straining field. The field coming from the experimental results is, of course, less smooth than the theoretical field, because of the measurement noise, but the stagnation point is clearly visible.

5. Conclusion

The velocity field near a viscous vortex ring core has been measured with the help of Particle Image Velocimetry. This field has been compared with theoretical models derived for thin core vortex rings in an ideal fluid. The results are in good agreement. The staining field, which is at the origin of the instability has been evidenced in the experimental results, demonstrating that the linear phase of the instability is not strongly influenced by the viscosity.

References

- [1] T. Maxworthy, The structure and stability of vortex rings, JFM 51 (1972) 15–32.
- [2] S.E. Widnall, J.P. Sullivan, S. Ezekiel, On the stability of vortex rings, Proc. Roy. Soc. A 332 (1973) 335–353.
- [3] S.E. Widnall, D.B. Bliss, C.Y. Tai, The instability of short waves on a vortex ring, JFM 66 (1974) 35–47.
- [4] S.E. Widnall, C.Y. Tsai, The instability of the thin vortex ring of constant vorticity, Philos. Trans. Roy. Soc. London Ser. A 287 (1977) 273–305.
- [5] P.G. Saffman, The number of waves on unstable vortex rings, JFM 84 (1978) 721–733.
- [6] L.E. Fraenkel, Examples of steady vortex rings of small cross-section in an ideal fluid, JFM 51 (1972) 119–135.